



Design, synthesis, and biological evaluation of a novel indoleamine 2,3-dioxygenase 1 (IDO1) and thioredoxin reductase (TrxR) dual inhibitor

Qing-Zhu Fan^{a,1}, Ji Zhou^{b,1}, Yi-Bao Zhu^a, Lian-Jun He^a, Dong-Dong Miao^a, Sheng-Peng Zhang^a, Xiao-Ping Liu^{a,*}, Chao Zhang^{a,*}

^a Center of Drug Screening and Evaluation, Wannan Medical College, Wuhu, Anhui 241000, PR China

^b Center for Reproductive Medicine, The First Affiliated Hospital of Wannan Medical College, Wuhu, Anhui 241000, PR China

ARTICLE INFO

Keywords:

IDO1
TrxR
Dual inhibitor
Antitumor

ABSTRACT

Targeting the Trp-Kyn pathway is an attractive approach for cancer immunotherapy. Thioredoxin reductase (TrxR) enzymes are reactive oxygen species (ROS) modulators that are involved in the tumor cell growth and survival processes. The 4-phenylimidazole scaffold is well-established as useful for indoleamine 2,3-dioxygenase 1 (IDO1) inhibition, while piperlongumine (PL) and its derivatives have been reported to be inhibitors of TrxR. To take advantage of both immunotherapy and TrxR inhibition, we designed a first-generation dual IDO1 and TrxR inhibitor (**ZC0101**) using the structural combination of 4-phenylimidazole and PL scaffolds. **ZC0101** exhibited better dual inhibition against IDO1 and TrxR *in vitro* and in cell enzyme assays than the uncombined forms of 4-phenylimidazole and PL. It also showed antiproliferative activity in various cancer cell lines, and a selective killing effect between normal and cancer cells. Furthermore, **ZC0101** effectively induced apoptosis and ROS accumulation in cancer cells. Knockdown of TrxR1 and IDO1 expression induced cellular enzyme inhibition and ROS accumulation effects during **ZC0101** treatment, but only reduced TrxR1 expression was able to improve **ZC0101**'s antiproliferation effect. This proof-of-concept study provides a novel strategy for cancer treatment. **ZC0101** represents a promising lead compound for the development of novel antitumor agents that can also be used as a valuable probe to clarify the relationships and mechanisms of cancer immunotherapy and ROS modulators.

1. Introduction

Combination drugs targeting multiple molecules are commonly used in cancer treatment to improve efficacy, decrease toxicity, and prevent the development of drug resistance [1]. A promising strategy that is gaining interest in drug discovery is the development of a single compound containing a combination of pharmacophores that are capable of modulating multiple targets simultaneously. This strategy of using a single multitargeted agent, called a “designed multiple ligand,” avoids the problems of complicated pharmacokinetic and pharmacodynamic relationships and drug–drug interactions associated with combination therapy [2].

L-tryptophan (L-Trp), which is the least abundant essential amino acid, can be metabolized via four distinct mechanisms: decarboxylation to tryptamine, protein synthesis, the serotonergic pathway, and the kynurenine (Kyn) pathway. Kyn pathway (KP) metabolism accounts for approximately 95% of all mammalian dietary Trp [3]. Indoleamine 2,3-dioxygenase (IDO1) is a heme enzyme that catalyzes the oxygenation of the indole ring of Trp to produce *N*-formylkynurenine (NFK) in the first rate-limiting step of the KP [4,5]. NFK is then metabolized to Kyn and its subsequent bioactive metabolites [6]. Tryptophan depletion results in inhibiting the proliferation of T lymphocytes, which are sensitive to low Trp levels. The production of KP metabolites can enhance immune tolerance by activating the aryl hydrocarbon receptor. Both contribute

Abbreviations: TLC, thin layer chromatography; THF, tetrahydrofuran; EA, ethyl acetate; DCM, dichloromethane; DMAP, 4-dimethylaminopyridine; LDA, lithium diisopropylamide; Boc, *t*-butyloxy carbonyl; DMF, dimethyl formamide; PE, petroleum ether; TFA, trifluoroacetic acid; IDO1, indoleamine 2,3-dioxygenase 1; TrxR, thioredoxin reductase; ROS, reactive oxygen species; PL, piperlongumine; L-Trp, L-tryptophan; Kyn, kynurenine; KP, kynurenine pathway; Trx, thioredoxin; NFK, *N*-formylkynurenine; PIM, 4-phenylimidazole; PI, propidium iodide; DCFH-DA, 2',7'-dichlorofluorescein diacetate; DMSO, dimethyl sulfoxide.

* Corresponding authors.

E-mail addresses: liuxiaoping@wnmc.edu.cn (X.-P. Liu), zhangchao@wnmc.edu.cn (C. Zhang).

¹ These authors contributed equally to this work.

<https://doi.org/10.1016/j.bioorg.2020.104401>

Received 13 March 2020; Received in revised form 12 October 2020; Accepted 17 October 2020

Available online 21 October 2020

0045-2068/© 2020 Elsevier Inc. All rights reserved.

to the immunosuppressed state of the tumor microenvironment [7,8]. In addition, evidence indicates that elevated levels of IDO1 expression in both tumor cells and antigen-presenting cells are correlated with a poor prognosis and reduced survival [9,10]. Given its important role in tumor immune escape, IDO1 represents a valuable therapeutic target in cancer immunotherapy.

More recently, thioredoxin reductase (TrxR) has been recognized as an attractive target for anticancer drug development [11]. Together with its substrate thioredoxin (Trx), TrxR maintains redox homeostasis in cells, preventing oxidative damage and mutations [12–14]. Both Trx and TrxR have been reported to be overexpressed in numerous cancer cells, and they have been observed to be associated with a poor prognosis and chemotherapy resistance [15–18]. The validity of TrxR as a target for anticancer treatment has been demonstrated by experiments showing that knockdown of TrxR in cancer cells brings about a reversal of tumor phenotype, as well as inhibition of DNA replication and cancer cell growth [19–21]. The Trx/TrxR system is a key component for maintenance of intracellular pathways involving redox homeostasis in mammalian cells. TrxR is upregulated in cancerous cells to combat reactive oxygen species (ROS) overproduction [22]. TrxR inhibition could modulate antioxidant levels and enhance intracellular ROS, and then disturb the cellular oxidative environment and induce cell death, thereby serving as a novel therapeutic agent. Notably, it has been shown that knocking down IDO1 using shRNA or IDO1 inhibitors heightens ROS levels, which in turn significantly inhibits cancer cell growth [23]. In the current work, we developed a novel small molecule that targets both IDO1 and TrxR.

4-phenylimidazole (PIM) has been reported to bind to a deep pocket of IDO1 with its phenyl ring oriented toward the lipophilic cavity, and its N-1 atom interacting with the heme iron [24,25]. Based on this finding, some derivatives have been reported that have improved activity at the micromolar level [26]. Piperlongumine (PL) is a natural product obtained from the fruit of the long pepper. PL is a form of traditional Chinese medicine that exhibits anticancer activity through a number of mechanisms, including inhibiting the phosphorylation of serine/threonine kinase Akt (Akt) [27] and blockade of both nuclear factor κ B (NF- κ B) and JAK-STAT3 signaling pathways [28,29]. PL has recently been reported to be a selective, irreversible inhibitor of TrxR that demonstrates antiproliferative activity against selected human cancer cell lines, with the Michael acceptor of PL postulated to react with a selenocysteine residue of the TrxR enzyme via a Michael addition reaction to form covalent adducts [30].

Since IDO1 inhibitors are generally developed as combination therapies with cytotoxic antitumor agents, radiotherapy, therapeutic vaccination, and other targeted therapies [9,31,32]. Our laboratory has focused on exploiting the combination of PIM and PL pharmacophoric scaffolds to produce novel single molecules that can improve anti-tumor effects both *in vitro* and *in vivo*, at least partly through simultaneous

inhibition of IDO1 and TrxR (Fig. 1). To our knowledge, there have been no other studies combining the key moieties to create a dual inhibitor for IDO1 and TrxR. Therefore, a novel phenylimidazole dihydropyridine derivative co-targeting IDO1 and TrxR was designed and synthesized to develop an effective anticancer agent exerting synergistic effects through an ROS-based mechanism and simultaneous activation of the antitumor immune response via IDO1 blockage.

2. Results and discussion

2.1. Chemistry

As shown in Scheme 1, compound ZC0101 was synthesized by using *tert*-butyl 4-(2-oxoethyl) piperidine-1-carboxylate as a starting material. The key intermediate **5** was obtained based on a previous reference [33]. Further reaction with bromoacetyl chloride yielded compound **6**. Treatment of **6** with PPh₃ in THF resulted in the quaternary phosphite, **7**. Compound **10** was synthesized via a coupling reaction using 2-formylphenylboronic acid and 4-iodo-1H-imidazole as the starting material. Subsequently, treatment of compound **10** with Boc₂O using DMAP as a base yielded another key intermediate, **11**. Finally, the target compound ZC0101 was obtained through a coupling reaction of compounds **7** and **11**, followed by deprotection of Boc. The structure of the target compound was confirmed by ¹H NMR and electrospray ionization mass spectrometry (ESI-MS). It was purified by silica gel column chromatography, and HPLC was used to determine its purity (>95%).

2.2. *In vitro* IDO1 and TrxR inhibitory activity evaluation

Initially, ZC0101 was evaluated for IDO1 inhibitory activity using recombinant human IDO1 as well as PIM (Aladdin, no. P135879, purity: 98%) and Epacadostat (MCE, no. HY-15689, purity: 99.95%) as reference drugs. As shown in Fig. 2A, ZC0101 exhibited potent IDO1 inhibitory activity with an IC₅₀ value in the nanomolar range, which was comparable to Epacadostat, but far superior to PIM.

The Docking results showed that the nitrogen of the imidazole in ZC0101 was directly bound to the heme iron which is similar to PIM and that the phenyl group was located at the expanded pocket A which is formed by Tyr126, Val30 and Gly262. Furthermore, it is predicted that the side chain dihydropyridinone occupied the pocket B which is composed of residues Arg231, Phe262, and Leu234 and the dihydropyridinone moiety took a position adjacent to Arg231 (Fig. 3). These docking results supported that the bulky hydrophobic group to fill pocket B of IDO1 is necessary for improving the IDO1 inhibitory activity [25]. Then, ZC0101 was evaluated for *in vitro* inhibitory activity against rat TrxR, with PL and Auranofin (MCE, no. HY-N2329 and HY-B1123; purity: 99.19% and 98%) as reference drugs. As shown in Fig. 2B, ZC0101 exhibited potent TrxR inhibitory activity, with an IC₅₀ value of 7.98 ± 0.02 μM, superior to that of PL at 21.9 ± 0.3 μM, while Auranofin showed more potent activity with an IC₅₀ value of 0.085 ± 0.002 μM. These observations demonstrate that ZC0101 acts as a dual enzymatic inhibitor *in vitro*.

2.3. Cellular cytotoxicity screening

We next performed cytotoxicity screening, which is summarized in Table 1. The cytotoxicity of ZC0101 was primarily investigated in non-small cell lung and colon cancer cells, with PL used as a reference drug, which was further compared to BEAS-2B (normal lung epithelial cells) and FHC (normal colon epithelial cells) in terms of IC₅₀ values. ZC0101 showed more cytotoxicity than PL in all screened cells, and especially in HCT-116 cells. In addition, both ZC0101 and PL could selectively kill cancer cells, although this selectivity was more obvious among FHC and tested colon cancer cells. Thus, follow-up cellular TrxR activity studies were mainly performed using HCT-116 cells.

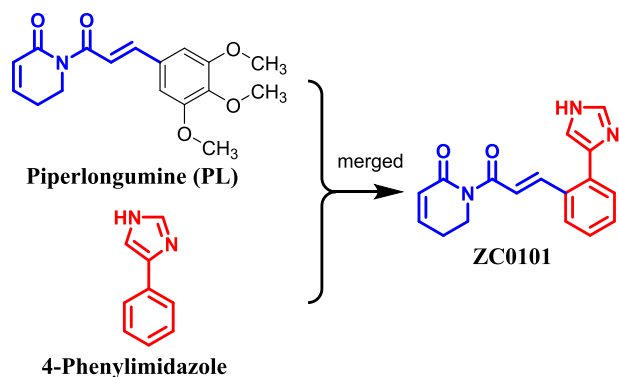
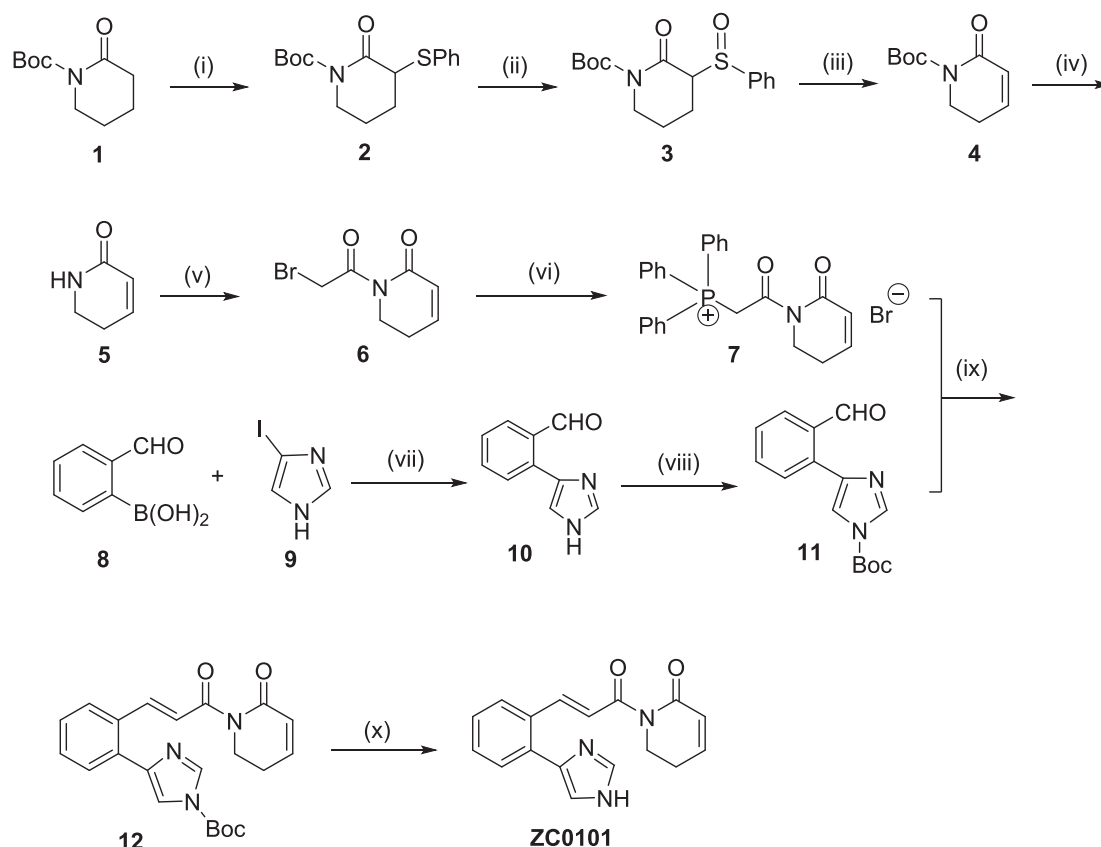


Fig. 1. Design of a novel inhibitor targeting thioredoxin reductase (TrxR) and indoleamine 2,3-dioxygenase (IDO1) by merging the TrxR inhibitor piperlongumine (PL) and the IDO1 inhibitor 4-phenylimidazole (PIM).



Scheme 1. Reagents and conditions: (i) LDA, THF, -78°C , PhSSPh, 50%; (ii) m-CPBA, DCM, NaHCO_3 ; (iii) Toluene, reflux, 80°C , two steps, 76%; (iv) DCM, TFA, 72%; (v) Bromoacetyl chloride, THF, rt., 20%; (vi) PPh_3 , THF, rt., 70%; (vii) DMF, $\text{Pd}(\text{PPh}_3)_4$, Na_2CO_3 , 40%; (viii) Boc_2O , DMAP, Et_3N , Toluene, rt., 65%; (ix) DMAP, CHCl_3 , rt., 50%; (x) CF_3COOH , rt., 72%.

2.4. Cellular IDO1 and TrxR inhibitory activity evaluation

To evaluate the IDO1 inhibitory activity of **ZC0101** in a cellular environment, a HeLa cell-based assay measuring Kyn was performed to calculate the EC_{50} of **ZC0101** as well as that of **PIM** and **Epacadostat** [34]. As shown in Fig. 2C, **ZC0101** had an EC_{50} of $1.41 \pm 0.01 \mu\text{M}$, which shows greater closeness to the EC_{50} of **Epacadostat** ($0.040 \pm 0.002 \mu\text{M}$) than the closeness between **PIM** ($>20 \mu\text{M}$) and **Epacadostat**. Additionally, **ZC0101** had an LC_{50} of $13.49 \pm 0.38 \mu\text{M}$ to HeLa cells as measured by cytotoxicity tests (Table 1), with a $\text{LC}_{50}/\text{EC}_{50}$ ratio of 9.6. This indicates that **ZC0101** effectively inhibited IDO1 activity in HeLa cells, and that the cell-based IDO1 activity was not caused by cytotoxicity. In addition, **ZC0101** treatment had almost no effect on IDO1 protein expression in HCT-116 and HeLa cells at low concentrations, while a high dose of **ZC0101** treatment reduced IDO1 protein expression in a concentration-dependent manner (Fig. 4B). Taken together, these findings show that **ZC0101** may inhibit cellular IDO1 in terms of both enzyme activity and protein expression.

To investigate whether **ZC0101** could effectively suppress TrxR activity in cancer cells, we first evaluated its cellular TrxR inhibition using an endpoint insulin reduction assay in HCT-116 cell lysates [35]. Treating HCT-116 cells with **ZC0101** led to a remarkable inhibition of cellular TrxR activity, with an IC_{50} of around $4.22 \mu\text{M}$, which was 2.5-fold lower than that of **PL** ($10.5 \mu\text{M}$, Fig. 2D). However, both **ZC0101** and **PL** exhibited weaker inhibitory activity than **Auranofin** (IC_{50} : $0.70 \pm 0.07 \mu\text{M}$, Fig. 2D). We also synthesized a TrxR probe, TRFS-green, developed by Fang et al [36]. By measuring and quantifying the fluorescence signal of this probe, we confirmed a greater decrease in TrxR activity in living HCT-116 and HeLa cells treated with **ZC0101** compared with cells receiving **PL** treatment (Fig. 4C-E). In addition, both **ZC0101** and **PL** treatment significantly suppressed TrxR protein

expression in HCT-116 and HeLa cells in a concentration-dependent manner, while cells treated with **ZC0101** had lower levels of TrxR than those treated with the same concentration of **PL** (Fig. 4A). Taken together, these results indicate that **ZC0101** showed better cellular TrxR inhibitory activity than **PL**.

2.5. Apoptosis analysis in cancer cells

To investigate whether the cell growth inhibition was associated with apoptosis, HCT-116 cells were treated with either DMSO or various concentrations of **ZC0101** and **PL** for 24 h. The cells were stained with Annexin-V and propidium iodide (PI), and the apoptotic ratio was determined by flow cytometry. As shown in Fig. 5, the percentages of apoptotic cells for **ZC0101** were 16.93% ($5 \mu\text{M}$), 30.34% ($10 \mu\text{M}$), and 46.46% ($20 \mu\text{M}$), respectively. The ability of **ZC0101** to induce apoptosis was stronger than that of **PL** (8.22%, 12.94%, and 27.16% at the same **PL** concentrations). Thus, we presumed that **ZC0101** exhibited better cancer cell growth inhibition than **PL** due to the combination of its better cell apoptosis-inducing activity and its superior cellular TrxR inhibitory activity.

2.6. RNA interference analysis in HCT-116 and HeLa cells

As we fully demonstrated that **ZC0101** inhibited both TrxR1 and IDO1 enzyme activity in both the *in vitro* assay and the cellular assay, we next questioned the physiological significance of TrxR1 and IDO1 inhibition on the cellular actions of **ZC0101**. We reduced TrxR1 or IDO1 expression in HCT-116 and HeLa cells by transfecting a siRNA specifically targeting TrxR1 or IDO1. The knockdown efficiency was validated in Fig. 6A and B. The suppression of both TrxR1 and IDO1 expression improved the effect of **ZC0101** treatment, as indicated by cellular

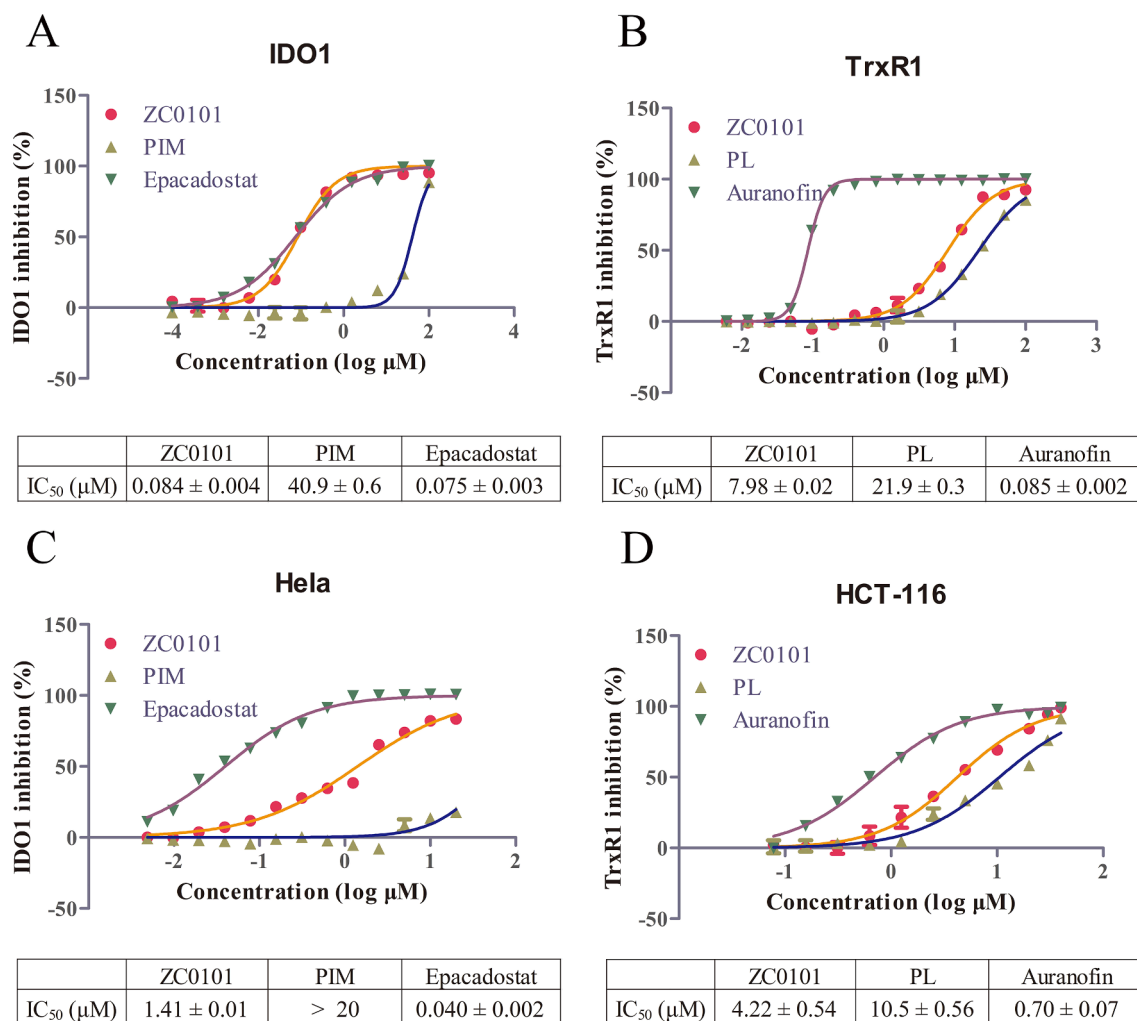


Fig. 2. ZC0101 inhibited both IDO1 and TrxR1 *in vitro*. (A, B) Concentration-effect curves for IDO1 and TrxR1 enzyme inhibitory activity of ZC0101. ZC0101 was more potent than PIM and PL in initial activity assays. (C) ZC0101 more effectively inhibited Kyn production than PIM in IFN- γ -treated human HeLa cells. (D) ZC0101 more effectively inhibited TrxR1 activity than PL in human HCT-116 cells. Dimethyl sulfoxide (DMSO) was used as the negative control. The results are expressed as the mean \pm standard deviation of three independent experiments.

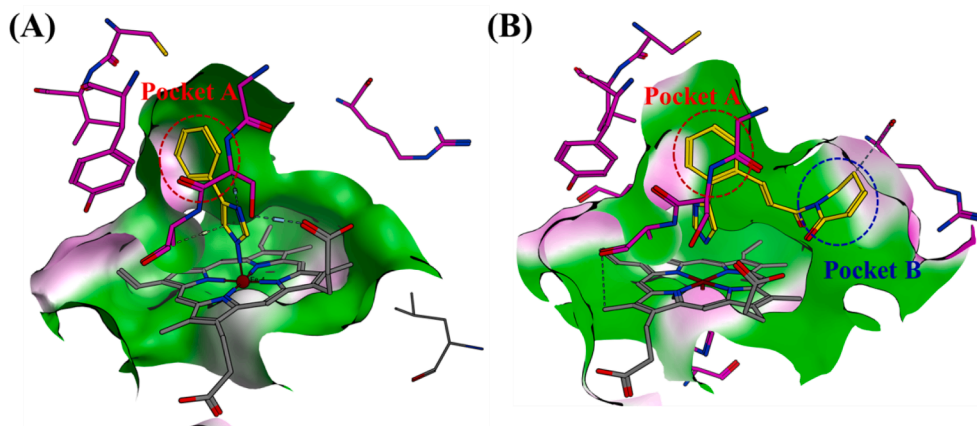


Fig. 3. (A) Binding mode of PIM in the IDO1 active site (PDB: 2D0T). (B) Proposed binding mode of compound ZC0101 in the IDO1 active site. Heme is rendered as a gray stick, IDO1 residues are shown as purple sticks, and compounds are shown as yellow sticks. (For interpretation of the references to color in this figure legend, the reader is referred to the web version of this article.)

enzyme assays. Knockdown of IDO1 expression did not improve ZC0101 treatment's anti-proliferation effect; in contrast, the effect was improved in cells with reduced TrxR1 expression (Fig. 6C). Taken together, our

loss-of-function data suggested that TrxR1 and IDO1 are cellular targets of ZC0101, and the anti-proliferation effect of ZC0101 is related to its inhibitory effect to TrxR1.

Table 1
Cytotoxicity screening of PL and ZC0101.

	Cell lines	IC ₅₀ (μM)	
		PL	ZC0101
Normal lung epithelial cells	BEAS-2B	17.12 ± 0.30	11.35 ± 0.21
Non-small cell lung cancer cells	A549	9.43 ± 0.12	7.34 ± 0.24
	A549/DDP	9.46 ± 0.11	7.65 ± 0.11
	H1299	5.28 ± 0.11	1.11 ± 0.01
	HCC827	6.30 ± 0.34	2.95 ± 0.12
	PC-9	6.63 ± 0.09	6.35 ± 0.16
Normal colon epithelial cells	FHC	46.90 ± 1.21	42.00 ± 0.27
Colon cancer cells	HCT-8	6.79 ± 0.03	0.44 ± 0.005
	HCT-8/5-Fu	3.77 ± 0.10	2.70 ± 0.55
	HCT15	3.54 ± 0.09	2.75 ± 0.07
	HCT116	6.68 ± 0.11	0.55 ± 0.24
	HT29	5.37 ± 0.30	1.31 ± 0.59
	SW620	8.66 ± 0.13	3.00 ± 0.07
Cervix cancer cells	HeLa	29.64 ± 0.74	13.49 ± 0.38

^aThe data (IC₅₀) were obtained through MTT assay and are expressed as the mean ± SD of three independent experiments.

2.7. ROS level analysis in HCT-116 and hela cells

The major function of TrxR1 is to maintain Trx in a reduced state, and thus defend against oxidative stress. IDO1 is also related to ROS production [23,37]. Having confirmed that ZC0101 is a potent TrxR1 and IDO1 dual inhibitor, we next determined the ROS levels in HCT-116 and HeLa cells. ROS levels were assessed by flow cytometry (Fig. 7A, B and E) and cell imaging (Fig. 7C and D) using the redox-sensitive fluorescent probe 2',7'-dichlorofluorescein diacetate (DCFH-DA). As shown in Fig. 7, treatment with ZC0101 for 4 h induced elevated ROS levels within HCT-116 and HeLa cells in a dose-dependent manner, indicating that ZC0101 had the ability to promote cellular ROS accumulation. Knocking down either TrxR1 or IDO1 expression could help to improve the ROS accumulation effect of ZC0101 treatment. These results demonstrated that the ROS accumulation effect of ZC0101 was related to its inhibitory effects to TrxR1 and IDO1.

2.8. Kynurenine/tryptophan metabolism study in mice

Inhibition of IDO1 activity *in vivo* could reduce plasma Kyn levels. To investigate whether ZC0101 could inhibit IDO1 *in vivo*, we performed a kynurenine/tryptophan metabolism study in C57BL/6 mice. Once daily oral dosing of Epacadostat or ZC0101 at 60 mg/kg reduced plasma kynurenine levels in mice, while the tryptophan levels were slightly upregulated (Fig. 8B). Additionally, the kynurenine/tryptophan ratio was also reduced (Fig. 8A). Taken together, these results indicated that ZC0101 was able to effectively suppress IDO1 activity *in vivo*.

3. Conclusions

In conclusion, due to the advantages of combining IDO1-targeted tumor immunotherapy and TrxR-targeted therapy, we hybridized PIM and PL into a single chemical entity. We synthesized and evaluated ZC0101, the first dual IDO1/TrxR inhibitor. ZC0101 exhibited better IDO1 and TrxR inhibitory activities than PIM and PL in both enzyme and cellular experiments. It also exhibited better cytotoxic activity than PL in all of the tested cancer cell lines and could significantly induce apoptosis in HCT116 cells, which was correlated with its strong *in vitro* TrxR inhibitory activity. In addition, ZC0101 also selectively killed colorectal cancer cells, while sparing normal colorectal cells. Furthermore, it induced ROS accumulation in cancer cells through its inhibitory effects to TrxR1 and IDO1. Considering the consistent results obtained from the cell-free and cell-based assays, this proof-of-concept study provides a novel strategy for the development of new antitumor agents. Thus, ZC0101 has potential as a promising lead compound for drug development. It can also be used a valuable probe to clarify the

relationships and mechanisms between cancer immunotherapy and TrxR-targeted therapy. However, structural optimization of ZC0101 and the synergistic effects of dual IDO1/TrxR inhibitors with immune checkpoint inhibitors (e.g., PD-1 antibodies) remain to be further investigated.

4. Experimental section

4.1. Chemistry

Reactions were monitored via thin-layer chromatography on silica gel plates (60F-254) visualized under UV light. Melting points were determined on a Mel-TEMP II melting point apparatus without correction. ¹H NMR and ¹³C NMR spectra were recorded in CDCl₃ on a Bruker Avance 300 MHz spectrometer at 300 MHz and 75 MHz, respectively. Chemical shifts (δ) are reported in parts per million (ppm) from tetramethylsilane (TMS) using the residual solvent resonance (CDCl₃: 7.26 ppm for ¹H NMR, 77.16 ppm for ¹³C NMR. Multiplicities are abbreviated as follows: s = singlet, d = doublet, t = triplet, q = quartet, m = multiplet). IR spectra were recorded on a Nicolet iS10 Avatar FT-IR spectrometer using KBr film. MS spectra were recorded on a LC/MSD TOF HR-MS Spectrum. Flash column chromatography was performed with 100–200 mesh silica gel, and yields refer to chromatographically and spectroscopically pure compounds.

Reactions and chromatography fractions were monitored on Merck silica gel 60F-254 glass TLC plates. All of the solvents were reagent grade and, when necessary, were purified and dried using standard methods.

4.1.1. Synthesis of 2-oxo-5,6-dihydropyridine-1 (2H) -tert-butyl carbonate (4).

First, 2-oxo-piperidine-1-tert-butyl carbonate **1** (3.98 g, 0.02 mol) was dissolved in anhydrous THF (20 mL), protected with N₂, cooled to –78 °C, after which LDA (20 mL) was slowly added in a dropwise manner, and stirred at –78 °C for 30 min. Diphenyl disulfide (4.36 g, 0.02 mol) was dissolved in anhydrous THF (40 mL). Under N₂ protection, the mixture obtained in the first step was slowly added thereto, and reacted at –78 °C for 1.5 h. After the reaction was complete, a saturated NH₄Cl solution was slowly added dropwise to the reaction system in order to quench the reaction. The solution was extracted three times with diethyl ether (3 × 100 mL) and saturated with NH₄Cl solution. Then, the organic layers were combined and dried over anhydrous MgSO₄, filter. The solvent was centrifuged to obtain the crude product, and column chromatography (PE/EA = 1: 10) was performed. The product **2** (3.10 g) was obtained as a colorless oil with a yield of 50%. ¹H NMR (DMSO-*d*₆): δ (400 MHz, CDCl₃) 1.52 (9H, s), 1.79–1.87 (1H, m), 1.97–2.12 (2H, m), 2.15–2.22 (1H, m), 3.67–3.74 (1H, m), 3.76–3.83 (1H, m), 3.85 (1H, t, *J* = 6.0 Hz), 7.28–7.32 (3H, m), and 7.52–7.55 (2H, m) ppm; ¹³C NMR (DMSO-*d*₆): δ_C (100 MHz, CDCl₃) 169.9, 153.3, 133.5, 129.1, 128.3, 83.2, 51.6, 45.9, 28.2, 20.8 ppm. HRMS (ESI): *m/z* calculated for C₁₆H₂₁NO₃SH⁺ (M + H⁺): 308.1315; found: 308.1320.

Next, 2-oxo-3-(phenylthio) piperidine-1-tert-butyl carbonate **2** (6.15 g, 0.02 mol) was dissolved in DCM (220 mL), and a saturated NaHCO₃ solution (41.5 mL) was added, then cooled to 0 °C. After that, m-CPBA (3.46 g, 0.02 mol) was added to the reaction system once and stirred at 0 °C for 2 h. At the end of the reaction, the organic layer was separated, and the aqueous phase was extracted three times with DCM (3 × 50 mL). The organic layers were combined, dried over anhydrous MgSO₄, filtered, and the solvent was rotary evaporated to obtain intermediate **3**. This was dissolved in toluene (10 mL) and refluxed at 80 °C for 3 h. After the reaction was completed, the solution was rotary evaporated, and the solvent was distilled off to obtain a crude product. Product **4** (2.98 g) was a colorless oily liquid with a yield of 76%. ¹H NMR (DMSO-*d*₆): δ (400 MHz, CDCl₃) 1.54 (9H, s), 2.40 (2H, td, *J* = 9.8, 1.9 Hz), 6.77 (1H, dt, *J* = 6.4 Hz, 1.8 Hz), 5.95 (1H, dt, *J* = 9.8, 1.9 Hz), 6.77 (1H, dt, *J* = 9.8, 4.2 Hz) ppm; HRMS(ESI): *m/z* calculated for C₁₀H₅NO₃H⁺ (M + H⁺): 198.1125; found: 192.1118.

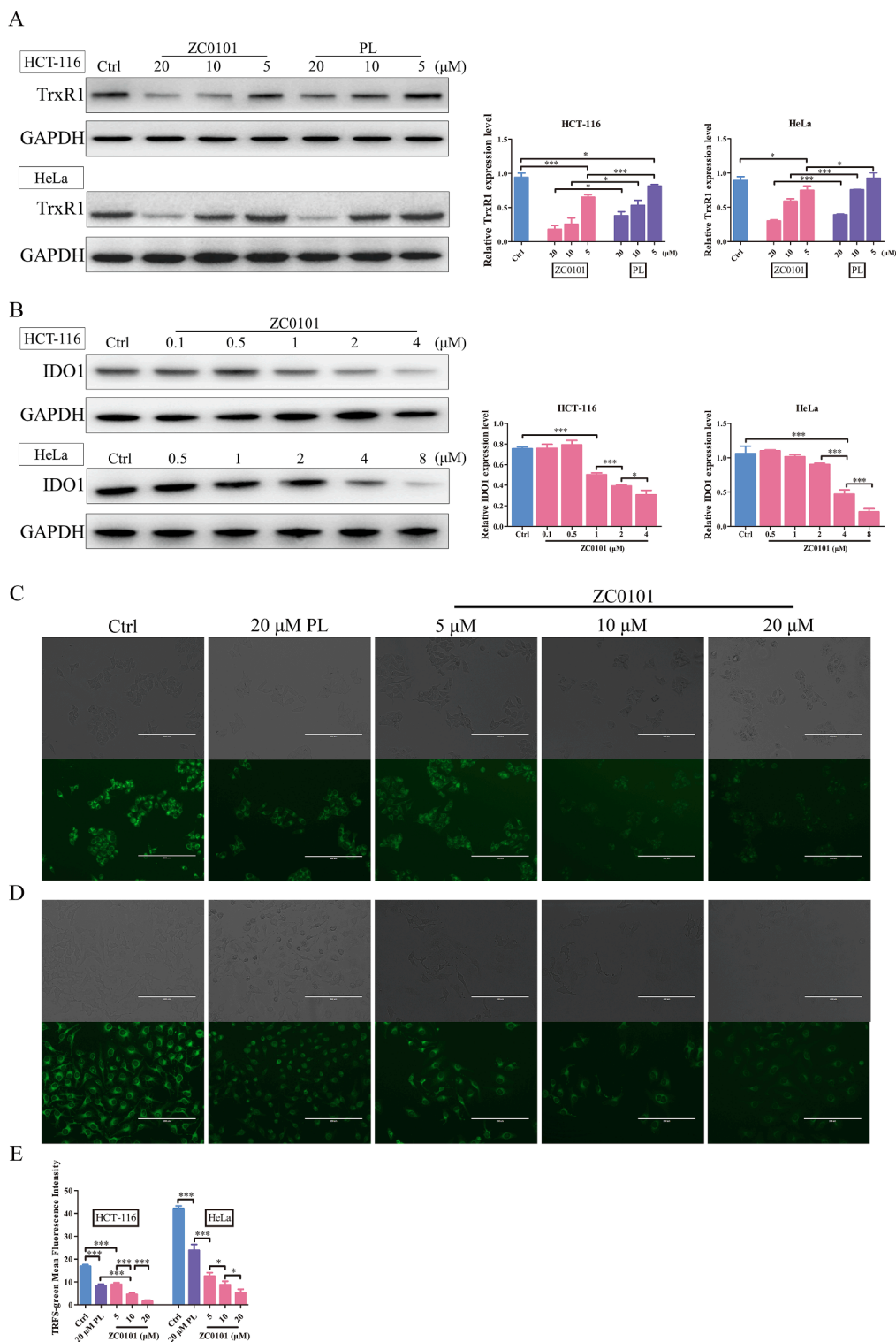


Fig. 4. Inhibitory effects of ZC0101 to IDO1 and TrxR1 in cancer cells. (A) ZC0101 exhibited better activity than PL in the downregulation of TrxR1 protein expression in HCT-116 and HeLa cells. (B) ZC0101 reduced IDO1 expression in HCT-116 and HeLa cells at high concentrations. Cells were treated with the indicated concentrations of ZC0101 or PL for 24 h, after which the cell extracts were prepared and analyzed by western blotting with an antibody against TrxR1. GAPDH was used as a loading control. TrxR1 proteins were quantified using ImageJ software and normalized to GAPDH. Data are expressed as the mean \pm standard deviation of three independent experiments. (C, D) Imaging of TrxR activity in living HCT-116 (C) or HeLa (D) cells. Cells were treated with the indicated concentrations of ZC0101 for 24 h followed by further treatment with TRFS-green (10 μM) for 4 h. Phase-contrast (top) and fluorescence (bottom) images were acquired by fluorescence microscopy (EVOS FL). PL (20 μM) and DMSO were used as the positive and negative controls. (E) TRFS-green mean fluorescence density was quantified using ImageJ. Mean fluorescence density = Integral fluorescence density / area. Data are expressed as the mean \pm SD of three independent experiments. Bars = SD. * $P < 0.05$, *** $P < 0.005$. (For interpretation of the references to color in this figure legend, the reader is referred to the web version of this article.)

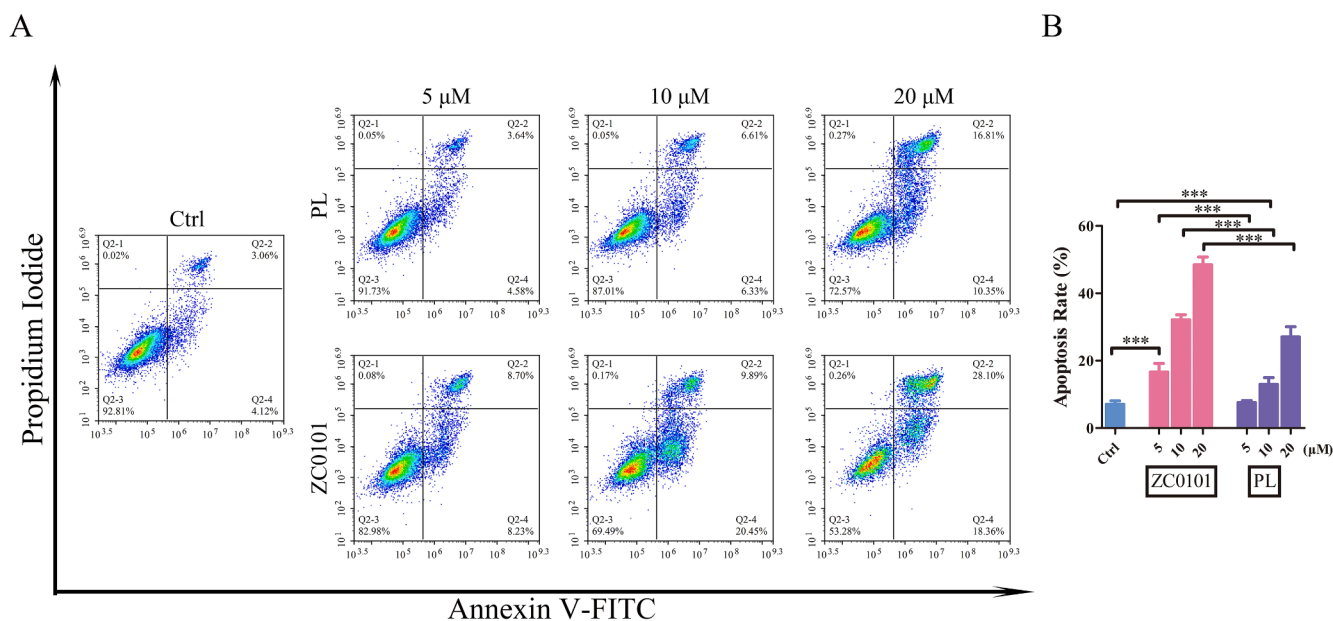


Fig. 5. ZC0101 showed more potency than PL in inducing cell apoptosis. (A) Analysis of apoptosis by Annexin-V/PI double-staining assay. HCT-116 cells were treated with ZC0101 or PL at indicated concentrations for 24 h. DMSO was used as the negative control. (B) The percentage of cell apoptosis was graphed by GraphPad Prism 5. The cells in Q2-2 and Q2-4 were considered apoptotic. Data are presented as the mean \pm SD values from at least three independent experiments. Bars = SD. *** P < 0.005.

4.1.2. Synthesis of 5,6-dihydropyridine-2 (1H) -one (5)

The 2-oxo-5,6-dihydropyridine-1 (2H) -*tert*-butyl carbonate **4** (2.87 g, 0.014 mol) obtained in the previous step was dissolved in dry DCM (18.2 mL) and cooled to 0 °C. TFA (14.35 mL, 0.12 mol) was slowly added dropwise. After the dropwise addition was completed, the ice bath was removed and the reaction was performed at room temperature for 2 h. Toluene (about 20 mL) was added to the reaction system, after which rotary evaporation was performed to remove toluene, DCM, and TFA. The residue was dissolved in DCM (50 mL), the organic phase was washed with saturated K_2CO_3 (40 mL), and the aqueous phase was repeatedly extracted (4 \times 50 mL) four times with DCM and methanol (approximately 10:1). The organic layers were combined and dried over anhydrous sodium sulfate (Na_2SO_4), followed by filtration and concentration by column chromatography (methanol: DCM = 1: 20) yielded product **5** (1 g) as a white solid with a yield of 72%. 1H NMR (DMSO- d_6): δ (400 MHz, $CDCl_3$) 2.32 (2H, tdd, J = 7.2, 4.2, 1.9 Hz), 3.40 (2H, td, J = 7.2, 2.7 Hz), 5.87 (1H, dq, J = 9.9, 1.9 Hz), 6.62 (1H, dt, J = 9.9, 4.2 Hz), 6.65 (1H, dq, br s) ppm; ^{13}C NMR (DMSO- d_6): δ_C (100 MHz, $CDCl_3$) 166.7, 141.6, 124.9, 39.6, 23.9 ppm. HRMS (ESI): m/z calculated for $C_5H_7NOH^+$ ($M + H^+$): 98.0600; found: 98.0559.

4.1.3. Synthesis of 1- (2-bromoacetyl) -5,6-dihydropyridine-2 (1H) -one (6)

5,6-Dihydropyridone (97 mg, 2 mmol) was placed in a single-necked flask under argon protection, dissolved in THF (6 mL), and 1.5 times equivalent NaH (0.12 g) was added at 0 °C, 3 mmol, then reacted for 1 h. Next, 1.2 times equivalent of bromoacetyl chloride (0.196 mL, 2.4 mmol) was added dropwise to the system. After the dropwise addition was completed, the mixture was returned to room temperature overnight. The progress of the reaction was monitored by TLC the next day (the developing solvent was EA and *n*-hexane in a ratio of 1:2). After the reaction was completed, 30 mL of saturated NH_4Cl was added, and then extracted three times with 30 mL of EA. After that, the aqueous phase was removed, and the organic phases were combined, dried over $MgSO_4$, filtered with suction, and concentrated. The concentrate was separated and purified by silica gel column chromatography (developing solvent was EA and PE in a ratio of 1:4), and the yield was 20%. 1H NMR (DMSO- d_6): δ (400 MHz, $CDCl_3$) 2.47 (2H, d, J = 4.2 Hz),

4.01–4.06 (2H, m), 4.60 (1H, s), 4.77 (1H, s), 6.02–6.05 (1H, m), 6.93–6.99 (1H, m). HRMS(ESI): m/z calculated for $C_7H_9BrNO_2H^+$ ($M + H^+$): 217.9817; found: 217.9826.

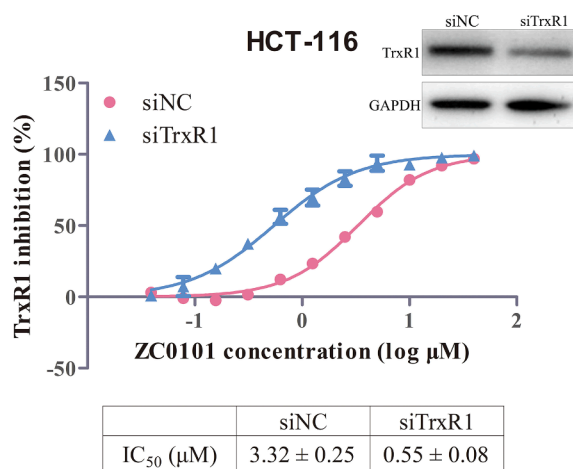
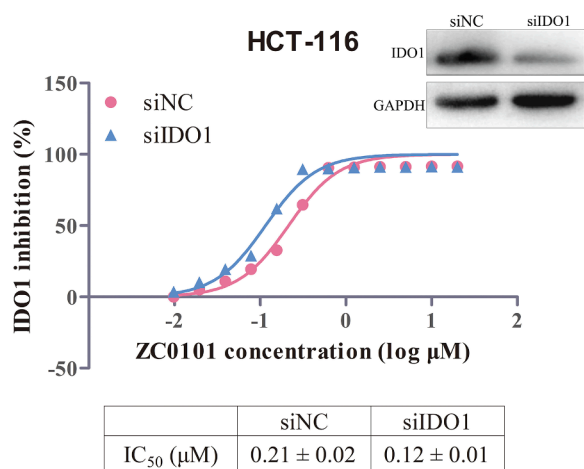
4.1.4. Synthesis of (2-oxo-2- (3,6-dihydropyridine-6-one) ethyl) triphenylphosphonium bromide (7)

Under the protection of argon, compound **6** (70 mg, 0.32 mmol) was dissolved in THF (1.25 mL), and then added to a THF system (0.75 mL) in which triphenyl phosphorus (83 mg, 0.32 mmol) was dissolved. This was then stirred at room temperature for 3–5 h. After the reaction was completed, the filtrate was discarded, and the filtered solid was washed with *n*-hexane and dried. The progress of the reaction was monitored by TLC (the developing solvent was EA and *n*-hexane in a ratio of 1:3). The yield was 70%. 1H NMR (DMSO- d_6): δ (400 MHz, $CDCl_3$) 2.59 (s, 2H), 3.87–3.91 (m, 2H), 5.97 (d, J = 8.0 Hz, 1H), 6.14 (d, J = 8.0 Hz, 2H), 6.99 (t, J = 4.0 Hz 1H), 7.73–7.92 (m, 15H). HRMS(ESI): m/z calculated for $C_{25}H_{23}BrNO_2P + H(M + H^+)$: 480.0728; found: 480.0716.

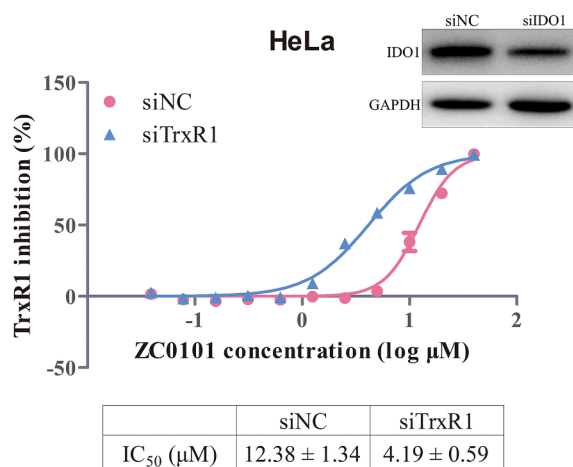
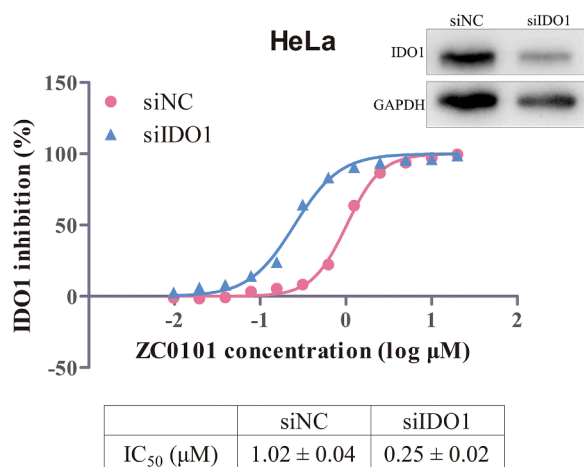
4.1.5. Synthesis of 2- (1H-imidazole-4-) benzaldehyde (10).

Next, 2-formylphenylboronic acid (0.6 g, 4 mmol), 4-iodo-1H-imidazole (0.485 g, 2.5 mmol), and tetrakis (triphenylphosphine) palladium (0.1445 g, 0.125 mmol) were dissolved in DMF (37.5 mL), then placed in a single-necked flask under the protection of argon. Saturated Na_2CO_3 (12.5 mL) was added and stirred at 110 °C. The progress of the reaction was monitored by TLC (the developing agent was 4:1 EA and *n*-hexane). After the reaction was completed, the reaction mixture was cooled to room temperature, after which 70 mL of water was added, and then extracted with 80 mL of EA three times. The aqueous phase was removed, and the organic phases were combined. After separation and purification on silica gel column chromatography (developing solvent was MeOH and DCM with a ratio of 75:2000), the reaction product was easy to tail in the developing agent. Adding an appropriate amount of triethylamine to the developing agent improved this phenomenon. The final product was 0.27 g with a yield of 40%. 1H NMR (DMSO- d_6): δ (400 MHz, $CDCl_3$) 7.33–7.43 (m, 1H), 7.66–7.78 (m, 4H), 7.82 (s, 1H), 10.53 (s, 1H), 12.46 (s, 1H). HRMS(ESI): m/z calculated for $C_{10}H_8N_2O + H(M + H^+)$: 173.0715; found: 173.0721.

A



B



C

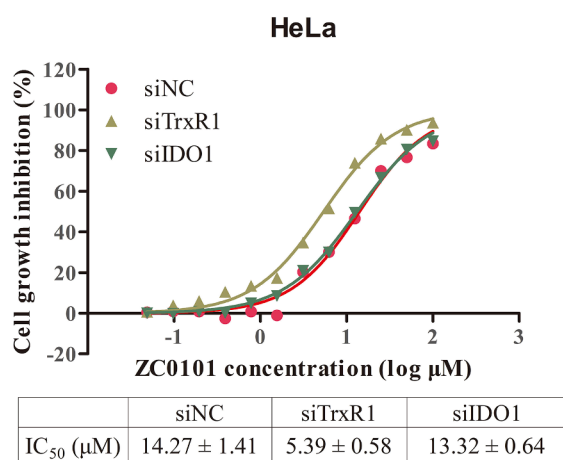
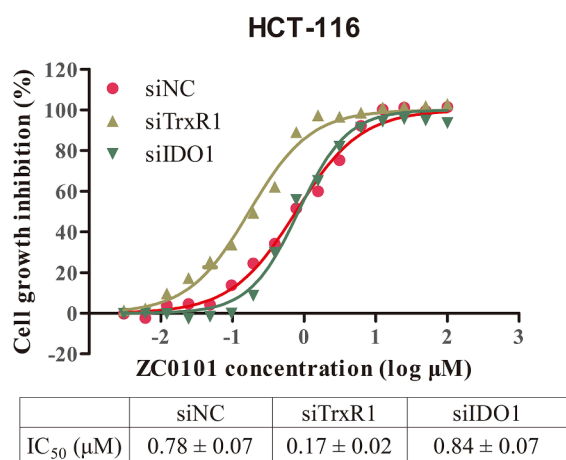


Fig. 6. The effects on ZC0101 activity after knockdown of TrxR1 or IDO1 expression. (A, B) Knockdown of TrxR1 and IDO1 expression improved the cellular enzyme inhibitory activity of ZC0101 treatment in HCT-116 (A) and HeLa (B) cells. Insets: the expression of TrxR1 or IDO1 was analyzed by western blotting. (C) Cytotoxicity of ZC0101 on HCT-116 and HeLa small interference RNA (siRNA)-transfected cells. The cells were transfected with indicated siRNAs for 36 h prior to ZC0101 exposure at the indicated concentrations for 24 h. Cell proliferation was determined by CCK-8 assay. Data are presented as the mean ± SD values from at least three independent experiments. Bars = SD.

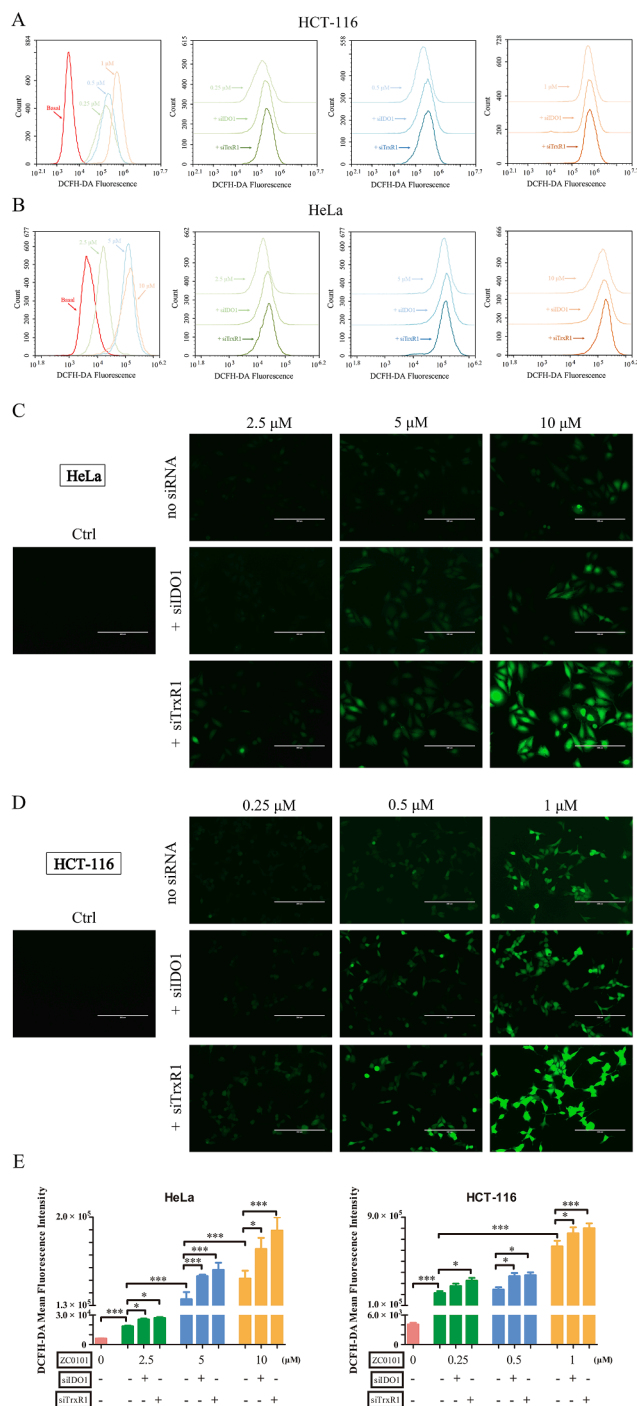


Fig. 7. ZC0101 induced intracellular ROS generation through its inhibitory effects to TrxR1 and IDO1. (A, B, C, D) Intracellular ROS generation induced by increasing doses of ZC0101. Cells were stained with 10 μ M DCFH-DA and ROS generation was improved by pre-transfection with siTrxR1 or siIDO1 for 56 h before exposure to ZC0101. Intracellular ROS generation in HCT-116 (A) or HeLa (B) cells was measured by flow cytometry. Fluorescence microscopy was also used to reveal the difference in ROS generation between HeLa (C) and HCT-116 (D) cells. (E) DCFH-DA mean fluorescence density was quantified by flow cytometry. Data are expressed as the mean \pm SD of three independent experiments. Bars = SD. * P < 0.05, ** P < 0.01, *** P < 0.005.

4.1.6. Synthesis of tert-butyl 4-(2-formylphenyl)-1H-imidazole-1-carboxylate (11)

Subsequently, 2-(1H-imidazole-4-) benzaldehyde (0.27 g, 1.57 mmol), 1.5 times the equivalent of Boc₂O (0.514 g, 2.36 mmol), 0.1

times the equivalent of DMAP (0.02 g, 0.16 mmol), and 1.5 times the equivalent of Et₃N (0.33 mL, 2.36 mmol) were dissolved in 23.5 mL of toluene, placed in a single-necked flask, and stirred at room temperature. The progress of the reaction was monitored by TLC (the developing solvents were EA and *n*-hexane in a ratio of 1:2). After the reaction was completed, the solvent was spin-dried. It was then separated and purified by silica gel column chromatography with EA and PE as the eluent at 1:4. The final product was 0.276 g with a yield of 65%. ¹H NMR (DMSO-*d*₆): δ (400 MHz, CDCl₃) 1.62 (s, 9H), 7.5 (t, J = 4.8 Hz, 1H), 7.72 (t, J = 4.8 Hz, 1H), 7.8 (t, J = 5.8 Hz, 2H), 8.15 (s, 1H), 8.38 (s, 1H), 10.41 (s, 1H). HRMS(ESI): m/z calculated for C₁₅H₁₆N₂O₃ + H(M + H)⁺: 273.1239; found: 273.1252.

4.1.7. Synthesis of (E)-1-(3-(2-(1H-imidazol-4-yl)phenyl)acryloyl)-5,6-dihydropyridin-2(1H)-one (ZC0101)

Compound **11** (17.2 mg, 0.1 mmol) and two equivalents of compound **7** (100 mg, 0.2 mmol) were dissolved in 1 mL of CHCl₃, after which three times the equivalent of DMAP (36.6 mg, 0.3 mmol) was added and stirred at room temperature for 4 h. Then, the system was stirred at 60 °C. The progress of the reaction was monitored by TLC (the developing solvent was EA and *n*-hexane in a ratio of 1:3). After the reaction, it was concentrated and subjected to silica gel column chromatography (the developing solvent was EA and *n*-hexane in a ratio of 1:6), and the yield was 50%. Compound **12** was dissolved in dry DCM (5 mL) and cooled to 0 °C. TFA was slowly added dropwise. After the dropwise addition was completed, the ice bath was removed and the reaction was performed at room temperature for 2 h. Toluene (about 10 mL) was added to the reaction system, and then rotary evaporation was performed to remove toluene, DCM, and TFA. The residue was dissolved in DCM (10 mL), the organic phase was washed with saturated K₂CO₃ (10 mL), and the aqueous phase was repeatedly extracted (4 \times 10 mL) four times with DCM and methanol (approximately 10:1). The organic layers were combined and dried over anhydrous sodium sulfate (Na₂SO₄), followed by filtration and concentration by column chromatography (methanol: DCM = 1:20) resulted in ZC0101 (20 mg) as a white solid with a yield of 72%. ¹H NMR (DMSO-*d*₆): δ (400 MHz, CDCl₃) 2.49–2.50 (m, 2H), 4.06 (t, J = 4.8 Hz, 2H), 6.07 (d, J = 4.8 Hz, 1H), 6.94–6.98 (m, 1H), 7.46 (t, J = 4.8 Hz, 1H), 7.49 (d, J = 7.2 Hz, 1H), 7.50 (t, J = 7.8 Hz, 2H), 7.74 (d, J = 5.6 Hz, 2H), 8.15–8.19 (m, 2H). ¹³C NMR (DMSO-*d*₆): δ_c (100 MHz, CDCl₃) 173.66, 170.66, 147.03, 144.58, 144.47, 141.05, 140.38, 135.56, 135.46, 133.96, 129.67, 127.12, 126.91, 122.54, 110.78, 46.79, 29.55 ppm. HRMS(ESI): m/z calculated for C₂₂H₂₃N₃O₄ + H(M + H)⁺: 293.1164; found: 293.1168.

4.2. Materials

Dimethyl sulfoxide (DMSO), L-Tryptophan, L-Kynurenine, sodium ascorbate, methylene blue, catalase from bovine liver, potassium phosphate monobasic, sodium hydroxide, trichloroacetic acid, 4-(Dimethylamino)benzaldehyde, human IFN- γ , NADPH, insulin, 5, 5'-dithiobis-2-nitrobenzoic acid (DTNB), ethylene diamine tetraacetic acid (EDTA), thioredoxin reductase from rat liver, and recombinant human thioredoxin (expressed in E.coli Trx) were purchased from Sigma-Aldrich (Darmstadt, Germany); a Cell Counting Kit-8 (CCK-8) was purchased from Dojindo Laboratories (Kumamoto, Japan); and rabbit polyclonal anti-TrxR1 antibody was purchased from Proteintech (#11117-1-AP; Wuhan, Hubei, China). Rabbit monoclonal anti-IDO1 antibody was purchased from Abcam (#ab211017, Cambridge, MA, USA). Mouse monoclonal anti-GAPDH antibody, HRP conjugated goat anti-rabbit and goat anti-mouse IgG (H + L) Secondary Antibodies were purchased from Thermo Fisher Scientific (#MA515738, 31,460 and 31430, respectively; Waltham, MA, USA). ROS assay kit and RIPA lysis buffer were purchased from Beyotime Institute of Biotechnology (#S0033 and P0013B; Haimen, Jiangsu, China). FITC-Annexin V Apoptosis Detection Kit I was purchased from BD Biosciences (#556547; San Jose, CA, USA). The Protease and Phosphatase Inhibitor Cocktail and BCA Protein Assay Kit

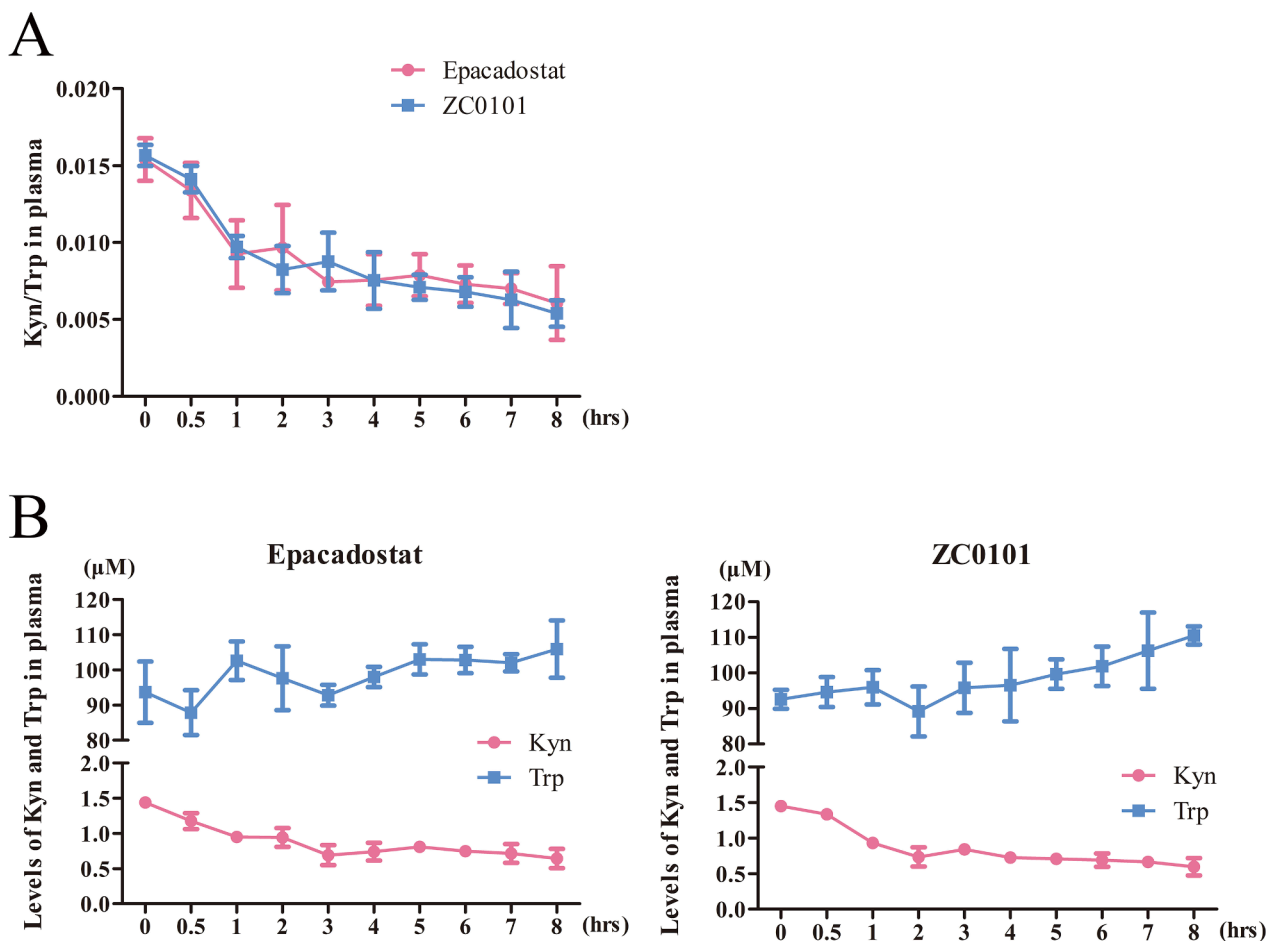


Fig. 8. ZC0101 efficiently suppressed Kyn in wild-type mice. (A, B) Wild-type male C57BL/6 mice were orally single administered Epacadostat or ZC0101 at 60 mg/kg, and blood was harvested at the indicated times. Plasma from five mice was analyzed for Kyn/Trp ratio (A), Kyn or Trp levels (B) by LC/MS/MS. The results were plotted as mean \pm SD.

were purchased from Thermo Fisher Scientific (#78440 and 23225, respectively; Waltham, MA, USA).

4.3. Cell culture

All of the human cell lines except A549/DDP and HCT-8/5-Fu were purchased from the American Type Tissue Culture Collection (ATCC, Manassas, VA, USA); A549/DDP was purchased from the China Infrastructure of Cell Line Resource (Beijing, China); and HCT-8/5-Fu was purchased from the Advanced Research Center of Central South University (Changsha, China). BEAS-2B cells were grown with BEGM medium (#CC-3170; Lonza, Walkersville, MD, USA) in the flasks pre-coated with a mixture of 0.01 mg/mL fibronectin (#F1056; Sigma-Aldrich), 0.03 mg/mL bovine collagen type I (#A1048301; Thermo Fisher), and 0.01 mg/mL bovine serum albumin (BSA, #A1933; Sigma-Aldrich). FHC cells were grown in DMEM/F12 medium (#30-2006; ATCC) with a final concentration of 25 mM HEPES, 10 ng/mL cholera toxin (#C8052; Sigma-Aldrich), 0.005 mg/mL insulin (#91077C; Sigma-Aldrich), 0.005 mg/mL transferrin (#T8158; Sigma-Aldrich), 100 ng/mL hydrocortisone (#HY-N0583; MCE, Monmouth Junction, NJ, USA), 20 ng/mL human recombinant EGF (#PHG0311; Thermo Fisher), and 10% (v/v) fetal bovine serum (FBS, #10099141C; Thermo Fisher). A549 and A549/DDP cells were grown in F12K medium; H1299, HCC827, PC-9, HCT-8, HCT-8/5-Fu, HCT-15, and HCT-116 cells were grown in RPMI-1640 medium; HT-29 cells were grown in McCoy's 5a modified medium; while SW620 cells were grown in Leibovitz's L-15 medium supplemented with 10% (v/v) FBS. HeLa cells were grown in Eagle's minimum essential medium

supplemented with 2 mM L-glutamine, 0.1 mM non-essential amino acids, 1 mM sodium pyruvate, and 10% (v/v) FBS. All of the cells except SW620 were maintained in a humidified atmosphere with 5% CO₂ at 37°C.

4.4. IDO1 enzyme assay

Recombinant human IDO1 (residues 5–403) with an N-terminal His tag (pET-28a-IDO1) was expressed in the *E. coli* BL21 (DE3) strain and purified by immobilized metal affinity chromatography (IMAC) with a protein purification system (AKTA pure 5, GE health, Uppsala, Sweden). The assays were performed at 37 °C using 0.625 μ M IDO1 and 0.2 mM L-Trp in the presence of 10 mM ascorbate, 10 μ M methylene blue and 0.1 mg/mL catalase in 50 mM potassium phosphate buffer (pH 6.5) for 1 h. Then, 140 μ L of the supernatant per well was transferred to a new 96 well plate. Subsequently, 10 μ L of 6.1 N trichloroacetic acid were mixed into each well and incubated at 60 °C for 30 min to hydrolyze the N-formylkynurenine produced by IDO1 to kynurenine. The reaction mixture was then centrifuged at 0 °C for 10 min with 10000 rpm to remove sediments. After that, 100 μ L of the supernatant per well were transferred to another 96 well plate and mixed with 100 μ L of 2% (w/v) 4-(Dimethylamino)benzaldehyde in acetic acid. The yellow color derived from kynurenine was measured at 480 nm using a Cytation 5 microplate reader (BioTek). L-Kynurenine, which was used as the standard, was prepared in a series of concentrations (200, 100, 50, 25, 12.5, 6.25, 3.12, and 1.56 μ M) in 100 μ L potassium phosphate buffer and analyzed through the same procedure. The percent inhibition at

individual concentrations was determined. The data were processed using nonlinear regression to generate IC_{50} values (Prism Graphpad 5).

4.5. TrxR1 enzyme assay

The TrxR activity was determined at room temperature using a microplate reader. The NADPH-reduced rat liver TrxR (0.24 μ g) was incubated with different concentrations of ZC0101, PL, or Aurofin for 1 h at room temperature (the final volume of the mixture was 50 μ L) in a 96-well plate. A master mixture in TE buffer (50 mM Tris-HCl pH 7.5, 1 mM EDTA, 50 μ L) containing DTNB and NADPH was added (final concentration: 2 mM and 200 μ M, respectively), and the linear increase in absorbance (AB) at 412 nm during the initial 3 min was recorded. The same amounts of DMSO (0.1%, v/v) were added to the control experiments, and the TrxR1 inhibitory rate was calculated using the following formula: TrxR1 inhibitory rate = $[1 - (AB \text{ value of test at 3 min} - AB \text{ value of test at 0 min}) / (AB \text{ value of control at 3 min} - AB \text{ value of control at 0 min})] \times 100\%$.

4.6. HeLa cell-based IDO1 activity assay [38–41]

HeLa cells were seeded in a 96-well culture plate at a density of 5×10^3 per well and grown overnight. On the next day, a final concentration of 10 ng/mL human IFN- γ , 15 μ g/mL L-Tryptophan, and serial dilutions of compounds in a total volume of 200 μ L culture medium per well were added into cells. After an additional 48 h of incubation, 140 μ L of the supernatant per well was transferred to a new 96-well plate. Then, 10 μ L of 6.1 N trichloroacetic acid were mixed into each well and incubated at 60 $^{\circ}$ C for 30 min to hydrolyze the *N*-formylkynurenine produced by IDO1 into kynurenine. The reaction mixture was then centrifuged at 0 $^{\circ}$ C for 20 min at 4000 rpm to remove sediments. After that, 100 μ L of the supernatant per well were transferred to another 96-well plate and mixed with 100 μ L of 2% (w/v) 4-(Dimethylamino)benzaldehyde in acetic acid. The yellow color derived from kynurenine was measured at 480 nm using a Cytation 5 microplate reader (BioTek). L-Kynurenine, which was used as the standard, was prepared in a series of concentrations (200, 100, 50, 25, 12.5, 6.25, 3.12, and 1.56 μ M) in 100 μ L HeLa cell culture media and analyzed using the same procedure. The percent inhibition at individual concentrations was determined. The data were processed using nonlinear regression to generate IC_{50} values (Prism Graphpad 5).

4.7. Cellular TrxR1 activity assay

After HCT-116 cells were treated with different concentrations of ZC0101, PL, and Aurofin for 24 h, the cells were harvested and washed twice with PBS. Total cellular proteins were extracted by RIPA buffer for 30 min on ice and quantified using the BCA procedure. TrxR1 activity in cell lysates was measured by the endpoint insulin reduction assay. In brief, the cell extract containing 20 μ g of total proteins was incubated in a final reaction volume of 50 μ L containing 100 mM Tris-HCl (pH 7.6), 0.3 mM insulin, 660 μ M NADPH, 3 mM EDTA, and 1.3 μ M E. coli Trx for 30 min at 37 $^{\circ}$ C. The reaction was terminated by adding 200 μ L of 1 mM DTNB in 6 M guanidine hydrochloride, pH 8.0. A blank sample, containing everything except Trx, was treated in the same manner. The absorbance (AB) at 412 nm was measured, and the blank value was subtracted from the corresponding absorbance value of the sample. The same amounts of DMSO were added to the control experiments, and the TrxR1 inhibitory rate was calculated using the following formula: TrxR1 inhibitory rate = $[1 - (AB \text{ value of sample} - AB \text{ value of blank}_{\text{sample}}) / (AB \text{ value of control} - AB \text{ value of blank}_{\text{sample}})] \times 100\%$.

4.8. Cell cytotoxicity screening

The effects of drug treatments on cell cytotoxicity were quantified using the CCK-8 assay. There were 5000 cells per well seeded in 96-well

plates overnight, and then treated with the drugs (PL and ZC0101: 100 μ M, 2-fold dilution for 12 concentrations). Complete, drug-free medium was added to the blank wells. Control cells were treated with DMSO only. After incubation for 24 h, 10 μ L CCK-8 was added to each well and cells were incubated at 37 $^{\circ}$ C for 4 h. Then, the medium was removed and 150 μ L DMSO was added, followed by gentle shaking. The absorbance (AB) at 450 nm was measured by a Cytation 5 microplate reader (BioTek), and the cell cytotoxicity inhibition rate was calculated using the following formula: Growth inhibition rate = $(AB \text{ value of control} - AB \text{ value of test}) / (AB \text{ value of control} - AB \text{ value of blank}) \times 100\%$.

4.9. Imaging TrxR activity in HCT-116 and HeLa cells using TRFS-green

Cells were treated with the indicated concentrations of ZC0101 or PL for 24 h followed by further treatment with TRFS-green (10 μ M) for 4 h. Phase contrast (top panel) and fluorescence (bottom panel) images were acquired by fluorescence microscopy (EVOS FL). Ten cells were randomly selected, and the fluorescence intensity in each individual cell was quantified using ImageJ software (version 1.8; NIH).

4.10. Western blot analysis

HCT-116 and HeLa cells were treated with ZC0101 or PL at the indicated concentrations for 24 h. The whole cells were lysed with RIPA lysis buffer. Protein quantification was performed using a BCA Protein Assay kit (#23225, Thermo Fisher Scientific), following which equal quantities of proteins (20 μ g) were separated via a 4–20% gradient SDS-PAGE gel, and transferred onto a PVDF membrane. The membranes were blocked with 5% BSA at room temperature for 2 h. TrxR1 and IDO1 antibodies were used at a 1:2000 dilution and GAPDH antibody was used at a 1:5000 dilution in 5% BSA together with the membranes, and incubated at 4 $^{\circ}$ C overnight. Following three washes in TBS/0.1% Tween 20, the membranes were each probed with secondary horseradish peroxidase-conjugated antibodies at a 10000-fold dilution in 5% BSA. Following six washes with TBS/0.1% Tween 20, the immune complexes were incubated with ECL reagents (#34577, Thermo Fisher Scientific), and detected using the ChemiDoc™ Touch Imaging System (Bio-Rad Laboratories, Hercules, CA, USA). The resulting bands on the membranes were calculated and normalized to GAPDH in each sample using ImageJ software.

To detect the knockdown efficiency of TrxR1 or IDO1, cells were pre-transfected with siTrxR1 or siIDO1 for 60 h prior to lysis.

4.11. Cell apoptosis assay

HCT-116 cells were plated in six-well plates at an initial density of 2.4×10^5 cells per well for 8 h in complete RPMI-1640 media. Cells were starved in serum-free RPMI-1640 medium for 16 h, followed by ZC0101 or PL treatment for 24 h. Cells were harvested, washed twice with phosphate-buffered saline (PBS, Thermo Fisher Scientific, Waltham, MA, USA), evaluated for apoptosis using the FITC-Annexin V Apoptosis Detection Kit I, and analyzed using the Novocyte flow cytometer (ACEA Biosciences, San Diego, CA, USA) with NovoExpress 1.2.4 software.

4.12. RNA interference analysis

TrxR1 siRNA, IDO1 siRNA, and a scramble nontargeting siRNA (siNC) were purchased from Biomics Biotech (Biomics Biotechnologies Co., Ltd., Nan Tong, China). The siRNA were transfected into cells using Lipofectamine 3000 reagents (Thermo Fisher, Waltham, MA, USA) according to the manufacturer's instructions. The siRNA sequences are as follows:

siTrxR1 sense: 5'- GCAUCAAGCAGCUUUGUUAdTdT-3'
 siTrxR1 antisense: 5'- UAACAAAGCUGCUUGAUGCdTdT-3'
 siIDO1 sense: 5'- CCUACUGUAUUCAGGCAAdTdT-3'
 siIDO1 antisense: 5'- UUGCCUUGAAUACAGUAGGdTdT-3'

For loss-of-function analysis, HCT-116 or HeLa cells were pre-transfected with siNC, siTrxR1, or siIDO1 for 36 h prior to ZC0101 exposure, followed by the same process as the CCK-8 assay, cellular TrxR1 and IDO1 activity assay.

4.13. Measurement of reactive oxygen species generation

Cellular ROS content was measured by flow cytometry and fluorescence microscopy for quantitative and qualitative evaluation. HCT-116 or HeLa cells were plated in six-well plates at a density of 2.0×10^5 cells/well and allowed to attach overnight, and then exposed to various concentrations of ZC0101 for 4 h (for HCT-116 cells: 0, 0.25, 0.5, and 1 μ M; for HeLa cells: 0, 2.5, 5, and 10 μ M). Cells were stained with 10 μ M DCFH-DA (Beyotime Biotech, Nantong, China) at 37 °C for 30 min, and then washed three times in serum-free medium. For flow cytometry, cells were collected and fluorescence was analyzed at excitation and emission wavelengths of 488 nm and 525 nm, respectively. Additionally, the mean value of DCFH-DA fluorescence intensity was utilized for quantitative analysis. For fluorescence microscopy, cells were collected and photos were obtained using the EVOS FL Imaging System (Thermo Fisher Scientific, Waltham, MA, USA). In the same experiments, cells were pretreated with siTrxR1 or siIDO1 for 56 h prior to ZC0101 exposure and ROS generation analysis.

4.14. Kynurenine/tryptophan measurement

All of the animal study procedures complied with the Wannan Medical College's Policy on the Care and Use of Laboratory Animals. All of the experiments were performed in accordance with the protocols approved by the Wannan Medical College Animal Policy and Welfare Committee. Eight-week-old male C57BL/6 mice were purchased from Cavens Lab Animal Inc. (Changzhou, Jiangsu, China) and administered a single oral dose of Epacadostat or ZC0101 (60 mg/kg), at which point food was removed from the cages. At various timepoints after dosing, mice were euthanized and blood was collected via cardiac puncture into pre-cold EDTA-3 K tubes. Blood sample was centrifuged at 4 °C (2000 g, 5 min) to obtain plasma within 15 min after sample collection. Then 50 μ L homogenized solution added with 200 μ L internal standard (500 ng/mL) in MeOH-1% trifluoroacetic acid. The mixture was vortexed for 5 min and centrifuged at 18000 rpm for 10 min. An aliquot of 5 μ L supernatant was injected onto the LC-MS/MS (API 4000) system. Linear assay ranges of 20 to 30,000 nM for kynurenine and 200 to 100,000 nM for tryptophan were demonstrated by analyzing 0.1 mL samples. Plasma samples were diluted 5-fold in water. Aqueous standards were prepared to alleviate the need for adjustment of endogenous tryptophan and kynurenine levels.

4.15. Statistical analysis

Results are presented as the mean \pm standard deviation (SD) of at least three independent experiments for each group. Statistical differences were determined by analysis of variance with Holm's post-hoc test for multiple comparisons, or by two sample *t* tests for independent samples using SPSS 22.0 software (IBM Corp., Armonk, IL, USA). All of the graphs were prepared using GraphPad Prism 5.0 (GraphPad; San Diego, CA, USA). *P* < 0.05 was considered to be statistically significant.

Declaration of Competing Interest

The authors declared that there is no conflict of interest.

Acknowledgements

This study was supported by the National Natural Science Foundation of China (Grant No. 81272485), the Natural Science Foundation of Anhui Province (Grant No. 1808085QH262), the Key Research and

Development Project of Anhui Province (Grant No. 202004a07020041), the University Natural Science Research Project of Anhui Province (Grant No. KJ2018A0259), the Major University Natural Science Research Project of Anhui Province (Grant No. KJ2019ZD30), the Foundation for Excellent Talents in Higher Education of Anhui Province (Grant No. gxbjZD18), the Specialized Research Fund for the Doctoral Program of Wannan Medical College (Grant No. rcqd201607), and the Key Research Cultivation Foundation of Wannan Medical College (Grant No. WK2017Z03).

Appendix A. Supplementary data

Supplementary data to this article can be found online at <https://doi.org/10.1016/j.bioorg.2020.104401>.

References

- [1] T.C. Chou, Theoretical basis, experimental design, and computerized simulation of synergism and antagonism in drug combination studies, *Pharmacol. Rev.* 58 (3) (2006) 621–681.
- [2] R. Morphy, Z. Rankovic, Designed multiple ligands. An emerging drug discovery paradigm, *J. Med. Chem.* 48 (21) (2005) 6523–6543.
- [3] L. Zhai, E. Ladomersky, A. Lenzen, B. Nguyen, R. Patel, K.L. Lauing, M. Wu, D. A. Wainwright, IDO1 in cancer: a Gemini of immune checkpoints, *Cell. Mol. Immunol.* 15 (5) (2018) 447–457.
- [4] A. Macchiarulo, E. Camaioni, R. Nuti, R. Pellicciari, Highlights at the gate of tryptophan catabolism: a review on the mechanisms of activation and regulation of indoleamine 2,3-dioxygenase (IDO), a novel target in cancer disease, *Amino Acids* 37 (2) (2009) 219–229.
- [5] S. Yamamoto, O. Hayaishi, Tryptophan pyrrolase of rabbit intestine. D- and L-tryptophan-cleaving enzyme or enzymes, *J. Biol. Chem.* 242 (22) (1967) 5260–5266.
- [6] A.B. Dounay, J.B. Tuttle, P.R. Verhoest, Challenges and opportunities in the discovery of new therapeutics targeting the kynurenine pathway, *J. Med. Chem.* 58 (22) (2015) 8762–8782.
- [7] D.H. Munn, M.D. Sharma, B. Baban, H.P. Harding, Y. Zhang, D. Ron, A.L. Mellor, GCN2 kinase in T cells mediates proliferative arrest and anergy induction in response to indoleamine 2,3-dioxygenase, *Immunity* 22 (5) (2005) 633–642.
- [8] A. Curti, S. TrabANELLI, V. Salvestrini, M. Baccarani, R.M. Lemoli, The role of indoleamine 2,3-dioxygenase in the induction of immune tolerance: focus on hematology, *Blood* 113 (11) (2009) 2394–2401.
- [9] C. Uytendhove, L. Pilotte, I. Theate, V. Stroobant, D. Colau, N. Parmentier, T. Boon, B.J. Van den Eynde, Evidence for a tumoral immune resistance mechanism based on tryptophan degradation by indoleamine 2,3-dioxygenase, *Nat. Med.* 9 (10) (2003) 1269–1274.
- [10] J. Godin-Ethier, L.A. Hanafi, C.A. Piccirillo, R. Lapointe, Indoleamine 2,3-dioxygenase expression in human cancers: clinical and immunologic perspectives, *Clinical cancer research : an official journal of the American Association for Cancer Research* 17 (22) (2011) 6985–6991.
- [11] J. Zhang, B. Zhang, X. Li, X. Han, R. Liu, J. Fang, Small molecule inhibitors of mammalian thioredoxin reductase as potential anticancer agents: An update, *Med. Res. Rev.* 39 (1) (2019) 5–39.
- [12] H.L. Ng, X. Ma, E.H. Chew, W.K. Chui, Design, synthesis, and biological evaluation of coupled bioactive scaffolds as potential anticancer agents for dual targeting of dihydrofolate reductase and thioredoxin reductase, *J. Med. Chem.* 60 (5) (2017) 1734–1745.
- [13] Y. Liu, D. Duan, J. Yao, B. Zhang, S. Peng, H. Ma, Y. Song, J. Fang, Dithiaarsanes induce oxidative stress-mediated apoptosis in HL-60 cells by selectively targeting thioredoxin reductase, *J. Med. Chem.* 57 (12) (2014) 5203–5211.
- [14] M. Bian, R. Fan, S. Zhao, W. Liu, Targeting the thioredoxin system as a strategy for cancer therapy, *J. Med. Chem.* 62 (16) (2019) 7309–7321.
- [15] S.J. Kim, Y. Miyoshi, T. Taguchi, Y. Tamaki, H. Nakamura, J. Yodoi, K. Kato, S. Noguchi, High thioredoxin expression is associated with resistance to docetaxel in primary breast cancer, *Clinical cancer research : an official journal of the American Association for Cancer Research* 11 (23) (2005) 8425–8430.
- [16] W. Peng, Z. Zhou, Y. Zhong, Y. Sun, Y. Wang, Z. Zhu, W. Jiao, M. Bai, J. Sun, H. Yin, J. Lu, Plasma activity of thioredoxin reductase as a novel biomarker in gastric cancer, *Sci. Rep.* 9 (1) (2019) 19084.
- [17] L. Xu, Y. Zhao, F. Pan, M. Zhu, L. Yao, Y. Liu, J. Feng, J. Xiong, X. Chen, F. Ren, Y. Tan, H. Wang, Inhibition of the Nrf2-TrxR axis sensitizes the drug-resistant chronic myelogenous leukemia cell line K562/G01 to imatinib treatments, *Biomed Res. Int.* 2019 (2019) 6502793.
- [18] B. Zhu, C. Ren, K. Du, H. Zhu, Y. Ai, F. Kang, Y. Luo, W. Liu, L. Wang, Y. Xu, X. Jiang, Y. Zhang, Olean-28,13b-olide 2 plays a role in cisplatin-mediated apoptosis and reverses cisplatin resistance in human lung cancer through multiple signaling pathways, *Biochem. Pharmacol.* 170 (2019) 113642.
- [19] L. Gan, X.L. Yang, Q. Liu, H.B. Xu, Inhibitory effects of thioredoxin reductase antisense RNA on the growth of human hepatocellular carcinoma cells, *J. Cell. Biochem.* 96 (3) (2005) 653–664.

- [20] M.H. Yoo, X.M. Xu, B.A. Carlson, V.N. Gladyshev, D.L. Hatfield, Thioredoxin reductase 1 deficiency reverses tumor phenotype and tumorigenicity of lung carcinoma cells, *J. Biol. Chem.* 281 (19) (2006) 13005–13008.
- [21] M.H. Yoo, X.M. Xu, B.A. Carlson, A.D. Patterson, V.N. Gladyshev, D.L. Hatfield, Targeting thioredoxin reductase 1 reduction in cancer cells inhibits self-sufficient growth and DNA replication, *PLoS ONE* 2 (10) (2007) e1112.
- [22] J. Zhang, X. Li, X. Han, R. Liu, J. Fang, Targeting the thioredoxin system for cancer therapy, *Trends Pharmacol. Sci.* 38 (9) (2017) 794–808.
- [23] D.J.M. Nguyen, G. Theodoropoulos, Y.Y. Li, C. Wu, W. Sha, L.G. Feun, T. J. Lampidis, N. Savaraj, M. Wangpaichitr, Targeting the kynurenine pathway for the treatment of cisplatin-resistant lung cancer, *Mol. Cancer Res.* 18 (1) (2020) 105–117.
- [24] S. Kumar, D. Jaller, B. Patel, J.M. LaLonde, J.B. DuHadaway, W.P. Malachowski, G. C. Prendergast, A.J. Muller, Structure based development of phenylimidazole-derived inhibitors of indoleamine 2,3-dioxygenase, *J. Med. Chem.* 51 (16) (2008) 4968–4977.
- [25] H. Sugimoto, S. Oda, T. Otsuki, T. Hino, T. Yoshida, Y. Shiro, Crystal structure of human indoleamine 2,3-dioxygenase: catalytic mechanism of O₂ incorporation by a heme-containing dioxygenase, *Proc. Natl. Acad. Sci. USA* 103 (8) (2006) 2611–2616.
- [26] T. Jiang, Y. Sun, Z. Yin, S. Feng, L. Sun, Z. Li, Research progress of indoleamine 2,3-dioxygenase inhibitors, *Future Med. Chem.* 7 (2) (2015) 185–201.
- [27] C. Zhang, L.J. He, Y.B. Zhu, Q.Z. Fan, D.D. Miao, S.P. Zhang, W.Y. Zhao, X.P. Liu, Piperlongumine inhibits Akt phosphorylation to reverse resistance to cisplatin in human non-small cell lung cancer cells via ROS regulation, *Front. Pharmacol.* 10 (2019) 1178.
- [28] H. Yuan, K.L. Houck, Y. Tian, U. Bharadwaj, K. Hull, Z. Zhou, M. Zhu, X. Wu, D. J. Tweardy, D. Romo, X. Fu, Y. Zhang, J. Zhang, J.F. Dong, Piperlongumine blocks JAK2-STAT3 to inhibit collagen-induced platelet reactivity independent of reactive oxygen species, *PLoS ONE* 10 (12) (2015) e0143964.
- [29] J. Zheng, D.J. Son, S.M. Gu, J.R. Woo, Y.W. Ham, H.P. Lee, W.J. Kim, J.K. Jung, J. T. Hong, Piperlongumine inhibits lung tumor growth via inhibition of nuclear factor kappa B signaling pathway, *Sci. Rep.* 6 (2016) 26357.
- [30] P. Zou, Y. Xia, J. Ji, W. Chen, J. Zhang, X. Chen, V. Rajamanickam, G. Chen, Z. Wang, L. Chen, Y. Wang, S. Yang, G. Liang, Piperlongumine as a direct TrxR1 inhibitor with suppressive activity against gastric cancer, *Cancer Lett.* 375 (1) (2016) 114–126.
- [31] A.J. Muller, J.B. DuHadaway, P.S. Donover, E. Sutanto-Ward, G.C. Prendergast, Inhibition of indoleamine 2,3-dioxygenase, an immunoregulatory target of the cancer suppression gene Bin1, potentiates cancer chemotherapy, *Nat. Med.* 11 (3) (2005) 312–319.
- [32] M. Li, A.R. Bolduc, M.N. Hoda, D.N. Gamble, S.B. Dolisca, A.K. Bolduc, K. Hoang, C. Ashley, D. McCall, A.M. Rojiani, B.L. Maria, O. Rixe, T.J. MacDonald, P. S. Heeger, A.L. Mellor, D.H. Munn, T.S. Johnson, The indoleamine 2,3-dioxygenase pathway controls complement-dependent enhancement of chemo-radiation therapy against murine glioblastoma, *J. Immunother. Cancer* 2 (2014) 21.
- [33] L.D. Sun, F. Wang, F. Dai, Y.H. Wang, D. Lin, B. Zhou, Development and mechanism investigation of a new piperlongumine derivative as a potent anti-inflammatory agent, *Biochem. Pharmacol.* 95 (3) (2015) 156–169.
- [34] M.F. Cheng, M.S. Hung, J.S. Song, S.Y. Lin, F.Y. Liao, M.H. Wu, W. Hsiao, C. L. Hsieh, J.S. Wu, Y.S. Chao, C. Shih, S.Y. Wu, S.H. Ueng, Discovery and structure-activity relationships of phenyl benzenesulfonylhydrazides as novel indoleamine 2,3-dioxygenase inhibitors, *Bioorg. Med. Chem. Lett.* 24 (15) (2014) 3403–3406.
- [35] J. Yao, D. Duan, Z.L. Song, J. Zhang, J. Fang, Sanguinarine as a new chemical entity of thioredoxin reductase inhibitor to elicit oxidative stress and promote tumor cell apoptosis, *Free Radic. Biol. Med.* (2020).
- [36] L. Zhang, D. Duan, Y. Liu, C. Ge, X. Cui, J. Sun, J. Fang, Highly selective off-on fluorescent probe for imaging thioredoxin reductase in living cells, *J. Am. Chem. Soc.* 136 (1) (2014) 226–233.
- [37] T. Majumdar, S. Sharma, M. Kumar, M.A. Hussain, N. Chauhan, I. Kalia, A.K. Sahu, V.S. Rana, R. Bharti, A.K. Halder, A.P. Singh, S. Mazumder, Tryptophan-kynurenine pathway attenuates beta-catenin-dependent pro-parasitic role of STING-TICAM2-IRF3-IDO1 signalosome in *Toxoplasma gondii* infection, *Cell Death Dis.* 10 (3) (2019) 161.
- [38] Y.H. Peng, S.H. Ueng, C.T. Tseng, M.S. Hung, J.S. Song, J.S. Wu, F.Y. Liao, Y.S. Fan, M.H. Wu, W.C. Hsiao, C.C. Hsueh, S.Y. Lin, C.Y. Cheng, C.H. Tu, L.C. Lee, M. F. Cheng, K.S. Shia, C. Shih, S.Y. Wu, Important Hydrogen Bond Networks in Indoleamine 2,3-Dioxygenase 1 (IDO1) Inhibitor Design Revealed by Crystal Structures of Imidazoleisoindole Derivatives with IDO1, *J. Med. Chem.* 59 (1) (2016) 282–293.
- [39] X. Feng, X. Qiu, H. Huang, J. Wang, X. Xu, P. Xu, R. Ge, X. Liu, Z. Li, J. Bian, Palladium(II)-Catalyzed Reaction of Lawsones and Propargyl Carbonates: Construction of 2,3-Furanonaphthoquinones and Evaluation as Potential Indoleamine 2,3-Dioxygenase Inhibitors, *J. Org. Chem.* 83 (15) (2018) 8003–8010.
- [40] Q. Du, X. Feng, Y. Wang, X. Xu, Y. Zhang, X. Qu, Z. Li, J. Bian, Discovery of phosphoramidate IDO1 inhibitors for the treatment of non-small cell lung cancer, *Eur. J. Med. Chem.* 182 (2019) 111629.
- [41] X. Feng, P. Shen, Y. Wang, Z. Li, J. Bian, Synthesis and in vivo antitumor evaluation of an orally active potent phosphoramidate derivative targeting IDO1/IDO2/TDO, *Biochem. Pharmacol.* 168 (2019) 214–223.